

White Matter Fiber Tractography via Anisotropic Diffusion Simulation in the Human Brain *

Ning Kang [†] Jun Zhang [‡]

Laboratory for High Performance Scientific Computing and Computer Simulation,
Department of Computer Science, University of Kentucky,
Lexington, KY 40506-0046, USA

Eric S. Carlson [§]

Department of Chemical Engineering, University of Alabama,
P. O. Box 870203, Tuscaloosa, AL 35487-0203, USA

and

Daniel Gembris

Institute for Computational Medicine, University of Mannheim,
B6, 23-29C, D-68131 Mannheim, Germany

July 27, 2004

*Technical Report No. 410-04, Department of Computer Science, University of Kentucky, Lexington, KY, 2004.

[†]The research work of this author was supported by the U.S. Department of Energy Office of Science under grant DE-FG02-02ER45961. E-mail: nkang2@cs.uky.edu.

[‡]The research work of this author was supported in part by the U.S. National Science Foundation under grants CCR-9988165, CCR-0092532, and ACR-0202934, in part by the U.S. Department of Energy Office of Science under grant DE-FG02-02ER45961, and in part by a University of Kentucky Research Support grant. E-mail: jzhang@cs.uky.edu, URL: <http://www.cs.uky.edu/~jzhang>.

[§]The research work of this author was supported by the U.S. Department of Energy Office of Science under grant DE-FG02-02ER45961. E-mail: ecarlson@bama.ua.edu.

Abstract

A new approach for noninvasively tracing brain white matter fiber tracts is presented using diffusion tensor magnetic resonance imaging (DT-MRI) data. This technique is based on successive anisotropic diffusion simulations over the human brain, which are utilized to construct three dimensional diffusion fronts. The fiber pathways may then be determined by evaluating the distance and orientation from fronts to their corresponding diffusion seeds. Real DT-MRI data are employed to demonstrate the tracking scheme. It is shown that several major white matter fiber pathways can be reproduced noninvasively, with the tract branching being allowed. Since the diffusion simulation, which is truly a physical phenomenon reflecting the underlying architecture of cerebral tissues, makes full use of the entire diffusion tensor data instead of part of it, our proposed approach is expected to enhance robustness and reliability in white matter fiber reconstruction.

Key words: fiber tractography, anisotropic diffusion simulation, diffusion tensor magnetic resonance imaging

1 Introduction

Diffusion tensor magnetic resonance imaging, or DT-MRI, is an extension of conventional MRI with the added capability of tracking and measuring the random motion of water molecules in all three dimensions, usually referred to as self-diffusion or “Brownian motion”. Since water diffusion is influenced by the microstructure, architecture, and physical properties of tissues, DT-MRI can render the information about how water diffuses in biological tissues containing a large number of fibers, like muscles or brain white matter, into intricate three-dimensional representations of tissue architecture. Thus, it can be exploited to visualize and extract information about the brain white matter and nerve fibers by using fiber pathways, which has raised promises for achieving a better comprehension of the fiber tract anatomy of the human brain. In fact, the general aim of using DT-MRI is the reconstruction of neural connectivity and the determination of fiber networks in the brain. In combination with functional MRI, it might potentially bring tremendous improvements in deeply understanding the crucial issue of anatomical connectivity and functional coupling between different regions of the brain [11, 15, 22, 24]. Therefore, the neuro-anatomical knowledge on connectivity interpreted from the DT-MRI information has been playing an indispensable role in neurosurgery planning [41] and in tackling brain diseases and disorders, such as Alzheimer’s disease [36, 39], attention-deficit hyperactivity disorder, and schizophrenia [1, 12].

It is known that water diffusion is anisotropic in brain white matter. The significant anisotropy presenting in white matter reveals microscopic properties of the anatomy of the nerve fibers by the fact that water tends to diffuse predominantly along the long axis of the fibers, because the longitudinally oriented structures, the dense packing of axons and the inherent axonal membranes, which are widely assumed to be the main barrier for water diffusion, hinder diffusion perpendicular to the fibers [6]. DT-MRI is sensitive to this anisotropy and is able to characterize it by non-invasively quantifying and assessing the self-diffusion of water *in vivo*. The information concerning the local orientation of fibers, extracted from the water anisotropic diffusion in white matter, forms the basis of utilizing DT-MRI to track fiber pathways and build connectivity mapping *in vivo*. The water diffusion behavior elucidated by the diffusion tensor imaging reflects the directional organization of the underlying white matter microstructure. DT-MRI characterizes the behavior on a voxel by voxel basis and for each voxel, the diffusion tensor yields the diffusion coefficient corresponding to any direction in space [2]. The direction of the greatest diffusion can be determined by evaluating the diffusion tensor in each voxel, which corresponds to the dominant axis of the white matter fiber bundles traversing the voxel.

A number of fiber tracking algorithms have been developed since the appearance of DT-MRI. The conventional white matter tractography reconstructs the pathways of white matter tracts by starting from a seed voxel and tracing down in a voxel-by-voxel manner, using an estimate of the local fiber orientation determined by the principal eigenvector in each voxel. At each voxel, the principal eigenvector, which is the one corresponding

to the largest eigenvalue generated by the eigen decomposition of the diffusion tensor, is aligned with the mean fiber direction in that voxel. Hence, trajectories can be produced by integrating the principal eigenvector field, which are expected to coincide with white matter fiber bundles. Attempts have been made to trace the neural fiber pathways in white matter tracts by this way [3, 11, 25, 38, 45, 46] and very impressive results on major fiber structures are exhibited. The approaches for fiber reconstruction based on this idea are sometimes referred to as streamline tracking techniques [23, 31], stemming from their similarity to computing flow streamlines from the velocity fields in fluid dynamics.

The streamline-based tracking technique is the one most commonly used in white matter tractography studies and it appears to give excellent results in many instances if the principal eigenvector field is smooth. However, it suffers from a couple of significant limitations. As noticed and summarized in [23, 34], the vector field is error prone in that the noise of DT-MRI data will influence the direction of the principal eigenvector, yielding an accumulation of orientational errors and thus an erroneous fork of the trajectory reconstruction process. Another major restriction is that it may also be affected by partial volume effects [43], leading to an unstable tracking of fibers through the primary eigenvector field. Since the current resolution of DT-MRI is 1-4 mm while the diameter of nerve fibers is in the magnitude of μm , in regions of fiber crossing, branching, or merging, the measured diffusion tensor data is difficult to interpret, which represents a complicated averaging of multiple compartments within a voxel, making the principal eigenvector field not adequate to describe such entangled structures.

A variety of methods have been proposed aiming to overcome the difficulties to which the streamline tracking technique is exposed, with more information incorporated from the diffusion tensor data. The method presented in [23, 42] improves the streamline approach by using the entire diffusion tensor to deflect the estimated fiber trajectory with an added deflection term. The schemes of [19, 34] use predefined knowledge to group together neighboring voxels based on a similarity measure and the resulting best neighbors in [34] lead to fiber trajectories while no trajectory information is provided in [19]. Taking into account the uncertainty of fiber direction, probabilistic and statistical approaches have been developed to study the cerebral connections by retrieving more of the information contained in the diffusion tensor. The method of [7] relies on regularized stochastic modeling. A statistical tracking algorithm based on linear state space models is presented in [14]. [29] creates the mapping of brain connections by means of the probabilistic Monte-Carlo method. The anatomical connectivity between brain regions is also assessed in [22] by a Monte-Carlo type algorithm, which is based on the macroscopic random walk with voxel to voxel jumps performed by a particle. The random walk algorithm developed in [16] improves the approach of [22], by which the brain connectivity can be modeled globally. Recently, level set theory, which models the evolution of an interface or front over time, is utilized to find the fiber paths connecting different brain regions. In [30, 31], the fast marching technique, based on level set principles, is applied in the context of fiber-tracking: For a given diffusion tensor field fronts are propagated to obtain time of arrival maps, which are then used to determine anatomical brain connectivity. Level set

theory has also been used in [9, 18] to implement a three dimensional geometrical flow to track the fiber bundles. There is a new magnetic resonance imaging technique worth mentioning, called q-ball imaging, which has the ability to resolve multiple axon directions within a single voxel [40].

As the measured quantity in DT-MRI is for water diffusion, an intuitive way to gain insights from the diffusion tensor data is to carry out a simulation of water diffusion, which is anisotropic and governed by the diffusion equation, over the brain. The white matter fiber bundles are assumed to proceed along the direction where the diffusion is the greatest. The fiber tracking method presented in this paper exploits the simulations of diffusion consisting of the solution of the anisotropic diffusion equation. The idea of studying brain connectivity by way of simulating the anisotropic diffusion has been preliminarily explored in [4, 13, 27], and [5] further extends the diffusion equation to a diffusion-convection equation by adding a convection term. However, in the above mentioned work based on this insight, there is no (or at best limited) attempt at determining the route of fiber pathways and connectivity between anatomical or functional regions in the brain, although the concentration or flow field over the brain is calculated and obtained. Our technique in the current paper relies on successive anisotropic diffusion simulations over the whole brain, which are utilized to construct three dimensional diffusion fronts. The next voxel, where a seed (an initial concentration value) will be placed, is located on the diffusion front which is created by the diffusion process initiated from the previous seed voxel. It is selected in terms of the fact that the faster the diffusion, the longer the distance will be traveled within the same amount of time, as well as the orientation information from itself and its neighboring voxels. The fiber pathways may then be determined by evaluating the distance and orientation of the vector from voxels on the fronts to their corresponding diffusion seeds.

The remainder of the paper is organized as follows. Section 2 illustrates the approach in detail for tracing fiber pathways by performing successive anisotropic diffusion simulations. The method is demonstrated by showing the tracking results with the human brain DT-MRI data in Section 3, including the white matter tracts generated in corpus callosum, the corticospinal tract, the optic radiation, and the inferior occipitofrontal fasciculus. In Section 4, potential advantages and disadvantages of the method are investigated and strategies for improvements are discussed. The final concluding remarks are given in Section 5.

2 Methodology

2.1 Data Acquisition and Processing

The diffusion tensor data used in the current paper to demonstrate the diffusion-based fiber tractography were acquired from a single healthy subject at the Institute for Medicine, Jülich Research Center, Jülich, Germany. A Siemens Magnetom Vision 1.5T scanner was used to do the measurement using single-shot spin-echo echo planar imaging with the

following parameters: $T_R = 15$ s; $T_E = 100$ ms; resolution: 96×128 ; plane orientation: transversal; Field of View (FoV): 240×240 mm²; slice thickness: 5 mm; number of slices: 16. The diffusion weighting corresponded to the Stejskal-Tanner gradient scheme [37] (b -factor: approximately 1000 s/mm²). The gradient direction angles ϕ_i and θ_j were chosen as multiples of 22.5° ($\phi_i = i \cdot 22.5^\circ$, $\theta_j = j \cdot 22.5^\circ$). For the suppression of eddy-current artifacts the employed sequence includes a zero and first order phase correction [8, 33]. The *non*-diffusion weighted images ($b = 0$ s/mm²) actually had a small diffusion weighting of about $b \approx 50$ s/mm², which was neglected in the computation of the diffusion tensors, but which is sufficient to significantly reduce sensitivity against blood flow changes.

During the actual data acquisition, the measurements were distributed over several pulse sequences (four different weightings per sequence: the first with $b = 0$ s/mm² and the other three with $b = 1000$ s/mm², but with three different gradient directions), which were repeated 10 times to increase the signal-to-noise ratio. This resulted in blocks of 4×10 data sets for each sequence. The averaging was performed in postprocessing with any potential head motion neglected (no motion compensation). The measurement was distributed over three sessions on different days. For the averaged data sets, however, a motion correction was performed using the SPM99 software package (<http://www.fil.ion.ucl.ac.uk/spm>), where the largest displacements were due to changes in head position between different sessions. The total measurement time was about eight hours including the latency times for image reconstruction that could not be postponed to the end of the measurement or performed off-line for technical reasons.

The resolution of the original calculated tensor data volume is $128 \times 128 \times 16$ with each voxel having the size $2.5 \times 2.5 \times 7.5$ mm³ defined on a Cartesian mesh. It has been interpolated by way of a continuous tensor field approximation technique developed and implemented in [28]. The data set after interpolation has dimensions of $128 \times 128 \times 48$, corresponding to a uniform voxel size of $(2.5 \text{ mm})^3$.

2.2 Anisotropic Diffusion in Brain

In our diffusion-based fiber tractography, we treat the whole 3D brain volume as an anisotropic physical system, over which a virtual water diffusion process is simulated. A thorough discussion about the diffusion process and related transport mechanisms in brain can be found in [26]. Anisotropic systems are those that exhibit a preferential spreading direction while isotropic systems are those that have no preference. According to Fick’s macroscopic law of diffusion, which illustrates the physical behavior of the diffusion process, the flux, J , is related to the concentration, C , by the equation

$$J = -D\nabla C, \tag{1}$$

where D is the so-called diffusion coefficient. This equation states that the concentration gradient ∇C causes the flux J which aims to compensate for this gradient. Plugging Equation (1) into the continuity equation

$$\frac{\partial C}{\partial t} + \nabla \cdot J = 0, \tag{2}$$

which expresses the conservation law of mass, we end up with the equation governing the general anisotropic diffusion process,

$$\frac{\partial C}{\partial t} = \nabla \cdot (D \nabla C), \quad (3)$$

where t is the independent time variable. This equation says that over the time, the rate of change in concentration is proportional to the divergence of the flux.

For a homogeneous isotropic environment, D is a scalar-valued constant and the directions of J and ∇C are parallel. In the presence of anisotropy, the flow field does not follow the concentration gradient directly. The diffusion coefficient D , therefore, has to be characterized as a second-order tensor, which delivers a complete description of the molecular mobility along each direction and the correlation between these directions. The diffusion tensor is represented by a three-by-three symmetric matrix, namely,

$$D = \begin{pmatrix} D_{xx} & D_{xy} & D_{xz} \\ D_{yx} & D_{yy} & D_{yz} \\ D_{zx} & D_{zy} & D_{zz} \end{pmatrix},$$

where the subscripts xx , xy , xz , etc., denote the values of the individual coefficients in the matrix that can be seen as the influence from directions in the input (being the concentration) on the various directions in the output (being the flux).

Since the brain tissue is not only anisotropic but also heterogeneous, the diffusion tensor D in such a case is space-dependent and thus the spatial derivatives of the tensor components D_{xx} , D_{xy} , D_{xz} , etc., must be introduced. In a Cartesian coordinate system, for a given position in the tensor volume, Equation (3) is written as

$$\begin{aligned} \frac{\partial C}{\partial t} = & \frac{\partial}{\partial x} \left(D_{xx} \frac{\partial C}{\partial x} + D_{xy} \frac{\partial C}{\partial y} + D_{xz} \frac{\partial C}{\partial z} \right) + \\ & \frac{\partial}{\partial y} \left(D_{yx} \frac{\partial C}{\partial x} + D_{yy} \frac{\partial C}{\partial y} + D_{yz} \frac{\partial C}{\partial z} \right) + \\ & \frac{\partial}{\partial z} \left(D_{zx} \frac{\partial C}{\partial x} + D_{zy} \frac{\partial C}{\partial y} + D_{zz} \frac{\partial C}{\partial z} \right). \end{aligned} \quad (4)$$

To provide an intuition for the tensor data, derived from the measured diffusion-weighted and diffusion-unweighted images, an axial slice of a diffusion tensor volume from the human brain is depicted in Figure 1. It shows a matrix of images, where each image is a color-coded representation of the corresponding component of the tensor matrix D .

2.3 Constructing Successive Diffusion Fronts

The fundamental idea behind our fiber tractography is to perform successive diffusion simulations over the brain stemming from a series of selected starting voxels where a seed (an initial concentration value) is placed. With certain thresholds satisfied, the starting voxels, or diffusion root nodes, are dynamically picked up from the nodes on the three dimensional diffusion interfaces or fronts produced by previous rounds of the diffusion simulation. Thus the first step to reconstruct fiber pathways starting from a pre-chosen root node $s \in \mathbb{R}^3$ (where \mathbb{R} is a set of real numbers) involves the simulation of diffusion

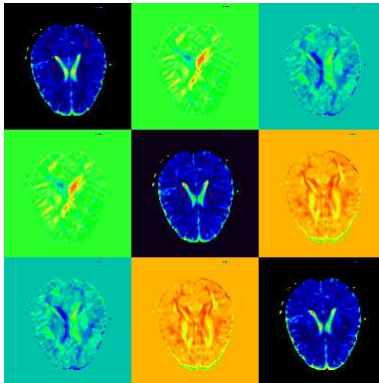


Figure 1: An axial slice of a diffusion tensor data volume, which shows the individual diffusion tensor components, corresponding to the diffusion tensor matrix D .

starting from a seed in this voxel. The virtual concentration seed of water spreads from the root node through neighboring nodes, within a limited amount of time, forming a diffusion front which is the surface of a diffusion volume containing nodes with non-zero¹ concentration values. The expansion of the diffusion volume originated from the root voxel is achieved by integrating the anisotropic diffusion equation (3) through the whole brain over a certain amount of time, subject to the following initial condition,

$$C \Big|_{t=0} = \begin{cases} 1 & \text{at the root voxel,} \\ 0 & \text{otherwise.} \end{cases} \quad (5)$$

For the boundary condition of Equation (3), we assume that the physical system containing the brain is insulated, i.e.,

$$(D\nabla C) \cdot \mathbf{n} = 0, \quad (6)$$

which corresponds to the von Neumann condition. This condition implies that the normal part of the gradient of the concentration on the boundary is zero, in other words, nothing escapes out of the domain.

The solution of the time-dependent diffusion equation (3) is not trivial since the human brain structure displays anisotropic, inhomogeneous diffusion properties. We have recently developed and implemented an unsteady state anisotropic diffusion solver framework, which is adapted to the cerebral circumstance and runs in both sequential and parallel computing environments [20, 21]. In the current paper, we solve sequentially the governing diffusion equation (3) by resorting to the established computational framework. Since the tensor data set used in the simulation is processed and stored on a Cartesian mesh, we do this by first discretizing the diffusion equation (4) on this grid using finite difference approximations. The central difference in space and the backward differentiation formula in time are applied to approximate the spatial derivative and time derivative

¹For zero concentration values, we actually mean values close to zero. A threshold can be applied to determine zero and non-zero values.

terms in Equation (4), respectively. The discretization of Equation (4) and its boundary condition (6) on the Cartesian grid generates a large scale system of semi-explicit differential-algebraic equations (DAEs). We then solve the initial value problem for the resulting system of DAEs by way of a high performance Implicit Differential-Algebraic (IDA) solver, using the scaled preconditioned GMRES (Generalized Minimal RESidual) iterative method with incomplete LU (Lower-Upper) factorization preconditioning applied. The IDA solver is one of the software packages contained in the ACTS (Advanced Computational Software) Collection (<http://acts.nersc.gov>).

In order to construct the diffusion front propagated from a root voxel where a seed has been placed, we only integrate over a fine-tuned amount of time the equation (4) through the whole brain using the time-dependent diffusion solver framework described above. The length of the integration time is determined in a way such that without the loss of revelations of the anatomical properties of the underlying nerve fibers, the number of voxels swept by the diffusion process initiated from the root voxel should be as small as possible. In fact, this value is chosen according to several factors including the magnitude of the tensor data, the spatial resolution of the computational grid, and the initial concentration at the root voxel. Once the time integration procedure is completed, a discrete approximation to the diffusion front can be calculated in terms of whether or not the concentration value is zero in a voxel. This is the ideal case though, we have to set a threshold to define zero concentration in the actual implementation. Thus all nodes in the computational grid can be partitioned into two groups, one with zero concentration value and the other with non-zero value. Let $V(r)$ denote the set of voxels that have non-zero concentration value, where r is the position of the root node. Since only a seed is diffused over the root node, the set $V(r)$ is comprised of the nodes in the diffusion-swept volume. For each member of $V(r)$, we consider its surrounding 6 closest neighboring nodes in a $3 \times 3 \times 3$ kernel. Let i, j, k index the relative coordinates of the 6 nearest neighbors to r with $i, j, k \in \{-1, 0, 1\}$. If $F(r)$ is the set of voxels that form the diffusion front of r , then for any node $p \equiv (p_x, p_y, p_z) \in V(r)$, we define

$$p \in F(r) \text{ if and only if } \begin{cases} \exists i, & (p_x - i, p_y, p_z) \notin V(r) \text{ or} \\ \exists j, & (p_x, p_y - j, p_z) \notin V(r) \text{ or} \\ \exists k, & (p_x, p_y, p_z - k) \notin V(r). \end{cases} \quad (7)$$

Figure 2 shows a simulated concentration distribution map of the anisotropic diffusion in the human brain by using the aforesaid diffusion tensor data. The simulated result is derived from solving the equation (4) under the initial condition (5) and boundary condition (6). The diffusion concentration map is overlaid on an image of the fractional anisotropy. Demonstrated in Figure 3 is an illustration of the discrete approximation to a diffusion front seed-diffused from a root voxel r .

Before presenting the algorithm to build up successive diffusion fronts originated from the start voxel s , we set up a queue Q , a first-in first-out data structure, to store and handle the dynamically produced front nodes. Q is initialized to the queue containing just the start node s , i.e., $Q = \{s\}$ before the start of the successive diffusion simulations;

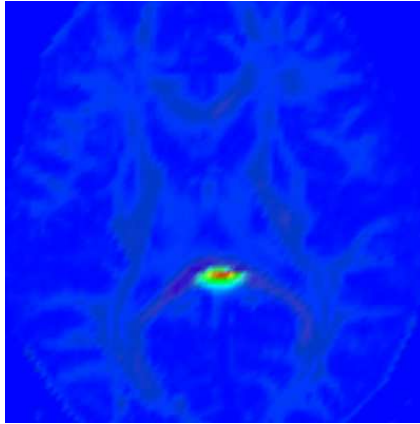


Figure 2: The concentration distribution map of the anisotropic diffusion originated from a starting voxel where a seed is placed. Shown here is the concentration field on a transversal cutting plane, superimposed on a map of the fractional anisotropy. The warmer colors (like red and yellow) represent larger concentration values, while the cooler colors (like blue and green) stand for smaller values.

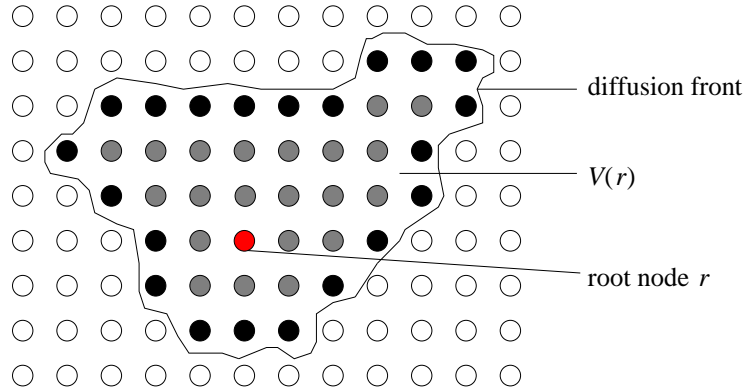


Figure 3: The illustration of the discrete approximation to a diffusion front, which borders the diffusion-swept volume $V(r)$ containing the node r (shown in red) as root where a seed is diffused and grey nodes with non-zero concentration value. Those originally grey nodes that satisfy the condition (7) are colored black, which are used to approximate the front. The white nodes are ones with zero concentration value.

thereafter, Q always contains the set of diffusion front nodes. We also define a set C to bear a number of criteria, which controls the way of determining the connection of fiber pathways. A detailed description of such a set C will be given shortly in section 2.4.

Once $F(r)$ is computed for the root node r , we further apply the criteria in C to the nodes of $F(r)$ and pick up those that meet the corresponding thresholds. We define $I(r)$ to be the set of nodes selected from $F(r)$ that are in accordance with those criteria in C , i.e.,

$$I(r) = \{ p \in F(r) \mid p \text{ meets all the criteria in } C \}. \quad (8)$$

$I(r)$ is then appended to the tail of the queue Q . The current head node of Q is removed off the queue and is considered to be a new root r' where a seed is diffused, and its diffusion front $F(r')$ is calculated in the same way as that of $F(r)$ by solving and integrating the equation (4) over a certain amount of time through the whole brain. As the derivation of $I(r)$, the set $I(r')$ is determined as well by checking up each member of $F(r')$ based upon the criteria in C , then it is added to the tail of Q . We continue in this way by repeatedly taking off the head node of Q and processing it as a new root to diffuse a seed over it, until the queue becomes empty. The following algorithm outlines the procedure for constructing successive diffusion fronts.

ALGORITHM 2.1 Construct successive diffusion fronts.

- 1 specify a start node s
- 2 initialize Q such that $Q = \{s\}$
- 3 **while** Q is not empty
- 4 remove the head node r off Q and take it as a root
- 5 get $V(r)$ by solving the anisotropic diffusion equation (4) with the initial and boundary conditions (5) and (6) imposed
- 6 compute $F(r)$
- 7 determine $I(r)$ and append it to the tail of Q
- 8 **end while**

2.4 Determining Fiber Pathways

During the construction of successive three dimensional diffusion fronts, the connection between a diffusion root node r and the nodes in its diffusion front $F(r)$ may determine the possible routes of the fiber tract going through both r and $F(r)$. As mentioned earlier, the connectivity is regulated by the criteria set C , which determines the members of $I(r)$. The fiber pathways passing the node r and its diffusion front can then be obtained by just connecting r and the nodes in $I(r)$. Obviously, fiber branching is thus achieved in this way since the size of the set $I(r)$ can be greater than 1 such that the tracking route is allowed to split at r .

There are seven criteria in C used to evaluate the information about distance and

orientation between the root r and its front nodes in $F(r)$. Let

$$C = \bigcup_{i \in \{1, \dots, 7\}} \{c_i\}.$$

The first criterion, c_1 , is the threshold for distance ratio (dr) measure, which is quantified as

$$dr = \frac{d}{d_{max}}, \quad (9)$$

where $d = \|\mathbf{v}(r)\|$ is the Euclidean distance in \mathbb{R}^3 of two points, connected by the vector $\mathbf{v}(r)$ pointing from r to a node in $F(r)$, while d_{max} is the maximum value among the d 's. The path reconstruction of white matter fiber bundles, which are assumed to proceed along the direction in which the diffusion is fastest, can be accomplished by our tracking approach thanks primarily to the fact that the faster the diffusion rate is, the longer the distance will be traversed within the same amount of time by the diffusion medium, water. If we just follow the direction with the longest distance, branching of fiber pathways cannot be handled adequately in the reconstruction. Moreover, both the error and noise in measurement and the partial voluming can deflect the tracking from the true path and orientation. In order to accommodate the branching tracts and minimize the possibility of deviation from the fiber trajectories, we set the threshold c_1 to be less than 1 and consider the cases with $dr \geq c_1$, following a few more directions with less fast diffusion rates rather than only the orientation with the fastest diffusion. By this way, the tracking procedure is likely to be more robust and reliable in noisy measurements.

We set the second criterion c_2 to be a threshold of an invariant anisotropy index, the fractional anisotropy (fa), which is defined as [32],

$$fa = \sqrt{\frac{(\lambda_1 - \lambda_2)^2 + (\lambda_2 - \lambda_3)^2 + (\lambda_3 - \lambda_1)^2}{2(\lambda_1^2 + \lambda_2^2 + \lambda_3^2)}}, \quad (10)$$

where λ_1 , λ_2 , and λ_3 (assuming $\lambda_1 \geq \lambda_2 \geq \lambda_3$) are the three eigenvalues of the 3×3 symmetric diffusion tensor D . fa assesses the fraction of the magnitude of D that can be attributed to anisotropic diffusion. It takes on values between 0 (fully isotropic diffusion) and 1 (infinite anisotropy). If the fa value of any voxel p falls below c_2 , p will not be considered as a diffusion root node, which restricts the paths tracking to the brain white matter and prevents erroneous trajectory propagation into the cerebrospinal fluid in the brain.

The next four criteria, from c_3 to c_6 , are called smoothness criteria which are used to judge the coherence of fiber directions along the reconstructed trajectories passing through r . The coherence measure depends on the inner products of four pairs of unit vectors (ip_1 , ip_2 , ip_3 , ip_4), which are expressed as

$$ip_1 = \hat{\mathbf{v}}(r) \cdot \hat{\mathbf{v}}(\pi(r)), \quad (11)$$

$$ip_2 = |\hat{\mathbf{v}}(r) \cdot \mathbf{e}_1(r)|, \quad (12)$$

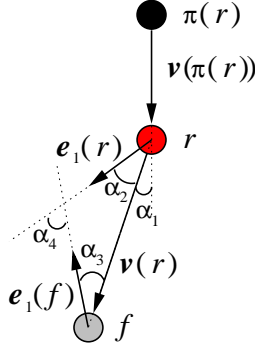


Figure 4: The transition smoothness of fiber trajectory relies on the size of the angles α_1 , α_2 , α_3 , and α_4 , which are determined by ip_1 , ip_2 , ip_3 , and ip_4 , respectively.

$$ip_3 = |\hat{\mathbf{v}}(r) \cdot \mathbf{e}_1(f)|, \quad (13)$$

$$ip_4 = |\mathbf{e}_1(r) \cdot \mathbf{e}_1(f)|, \quad (14)$$

where $\hat{\mathbf{v}}(r)$ and $\hat{\mathbf{v}}(\pi(r))$ are normalized vectors,

$$\hat{\mathbf{v}}(r) = \frac{\mathbf{v}(r)}{\|\mathbf{v}(r)\|}, \quad \hat{\mathbf{v}}(\pi(r)) = \frac{\mathbf{v}(\pi(r))}{\|\mathbf{v}(\pi(r))\|}.$$

Here, $\pi(r)$ is called the predecessor voxel of r , i.e., $r \in I(\pi(r))$, and $\mathbf{v}(\pi(r))$ is the vector pointing from $\pi(r)$ toward r . $\mathbf{e}_1(r)$ and $\mathbf{e}_1(f)$ are the principal eigenvectors (corresponding to the largest eigenvalue λ_1 of the diffusion tensor D) at the voxel r and $f \in F(r)$, respectively. c_3, \dots, c_6 are the thresholds for ip_1, \dots, ip_4 , respectively. Indeed, ip_1, \dots, ip_4 measure the angles between orientations of those vectors, as shown in Figure 4, and the equations from (11) to (14) also imply that $ip_1 \in [-1, 1]$ and $ip_2, ip_3, ip_4 \in [0, 1]$. Since $\mathbf{v}(\pi(r))$ is an established vector implying the presence of a trajectory passing in this direction, the information contained in ip_1 is exploited to appraise the next possible fiber path orientation aligned with $\mathbf{v}(r)$ by examining the degree of co-linearity between $\mathbf{v}(\pi(r))$ and $\mathbf{v}(r)$. The tracking direction is able to be pushed forward consistently and smoothly without erratically turning backward by setting a higher threshold value for ip_1 . Furthermore, the thresholds for ip_2, ip_3 , and ip_4 ensure that the currently computed fiber tract, presented by $\mathbf{v}(r)$, is directionally coherent with the local fiber orientation at r as well as with the local fiber orientation at f .

The last criterion, c_7 , is the maximum number of voxels $I(r)$ allowed to have if there are more voxels than expected satisfying all previous six criteria. The elements of $I(r)$ are determined by checking each voxel in $F(r)$ in a non-ascending order of the distance ratio to see if it meets all aforementioned six criteria until the prescribed capacity of $I(r)$ is reached. The purpose of setting this threshold is to put in control the overall computation time for doing the successive diffusion simulations.

Aimed at recovering the fiber pathways after the construction of diffusion fronts, each voxel p in the voxel grid owns a memory of its predecessor voxel, $\pi(p)$, where $p \in I(\pi(p))$.

In the current implementation of our tracking scheme, $\pi(p)$ is the sole predecessor of p if there is one. Thus, back propagation from the voxels on diffusion fronts by following continuously the corresponding predecessor voxels may lead to paths that merge to the start voxel s . This merging corresponds to the procedure that can be viewed in the reverse direction as fiber tracts branch outwards from s . By combining Algorithm 2.1 with the back propagation process, our diffusion simulation based fiber tracking algorithm is presented as follows.

ALGORITHM 2.2 Fiber tracking by diffusion simulations.

- 1 specify a start voxel s
- 2 build successive diffusion fronts (Algorithm 2.1)
- 3 record π values for voxels during front construction
- 4 retrieve fiber pathways using back propagation

3 Results

In this section, we present a number of experimental results obtained by noninvasively tracing fiber bundles in the human brain with our diffusion-simulation based fiber tracking algorithm. All the reconstructed fiber trajectories launched from different regions of interest are projected and superimposed on maps of the fractional anisotropy (fa). Figure 5 draws an axial slice of the color-scaled fa map, which shows white matter tracts as warmer colors (high signal intensity) reflecting that water diffusion is highly anisotropic in these directionally organized tissue structures. A view of the principal eigenvectors of the diffusion tensor in an axial slice of brain is depicted in Figure 6, which is projected onto the corresponding fa map as shown in Figure 5. The eigenvector map further illustrates the highly directional nature of the white matter structures.

In all the conducted experiments, we have set the threshold values for the criteria contained in C as follows. The threshold for distance ratio measure, c_1 , is chosen to be 0.75, below which we stop processing more voxels on the diffusion front. We evaluate the fa value by setting c_2 to be 0.2 that proved to reliably prevent the algorithm from entering grey matter structures and cerebrospinal fluid in the ventricles and around the brain. We set $c_3 = 0.7$, i.e., the angle between vectors $\mathbf{v}(r)$ and $\mathbf{v}(\pi(r))$ must be no more than approximately 45° , to keep the tracked fiber path from sharp transition. The thresholds for ip_2 , ip_3 , and ip_4 use the same value, $c_4 = c_5 = c_6 = 0.85$, to guard the local directional coherence of the estimated fiber tract and curb the trajectory from following unlikely pathways. It follows that the acute angle between any two of the three involved vectors, $\mathbf{v}(r)$, $\mathbf{e}_1(r)$, and $\mathbf{e}_1(f)$, is not allowed to exceed 32° . c_7 is set to be 5, which implies that $I(r)$ is able to hold up to five voxels.

We demonstrate the diffusion based tracking approach by exploring its ability to reproduce the well-known course of white matter structures. The first of the fiber pathways considered as an example of the method is the corpus callosum tract, which interconnects

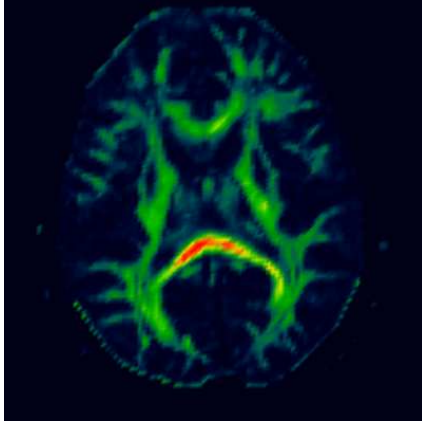


Figure 5: A transversal slice of the fractional anisotropy (fa) map in color scale, where the smallest values are colored blue; green corresponds to values near the middle of the scale and red to the largest values.

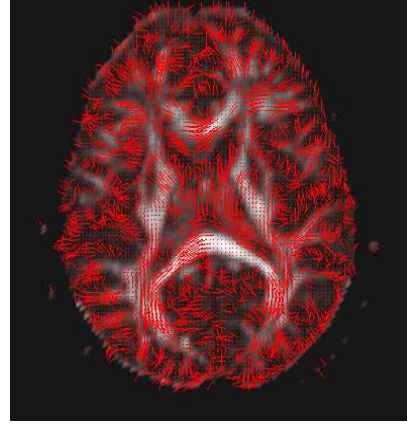


Figure 6: A cross-section image of principal eigenvectors, which are projected onto a fractional anisotropy (fa) map (grey scale) and depicted as red needles.

the left and right cerebral hemispheres and has the highest anisotropy and temperate curvature. Figure 7 shows the reconstructed fiber tracts stemmed from two start voxels located in the anterior and posterior portions of the corpus callosum, i.e., the genu and splenium, respectively. The tracking from the two start voxels results in fibers traversing the genu and splenium and running toward the frontal and occipital poles of the two cerebral hemispheres, respectively. The trajectories are traced in parallel to the curvature of the genu and splenium, exhibiting an arched shape, which is consistent with the known anatomy. It is evident from Figure 7 that our diffusion based tracking scheme allows for tract branching since the generated fiber trajectories start from a single point and then end up with multiple points, forming a number of branching pathways from one single start voxel. The corpus callosum commissural fibers calculated here are similar to those obtained in [3, 11, 23, 45].

The next example of the fiber tract reconstructed by our technique belongs to the system of projection pathways, which connects the cerebral cortex and the spine. More specifically, we attempt to generate the fiber pathways for the corticospinal tract, which conveys impulses for cortical control of the voluntary movements. The tracking result of the projection traces is elucidated in Figure 8. The estimate of this type of corticofugal fiber bundles is obtained by launching trajectories from a single start voxel placed approximately in the left portion of the base of the pons area, similar to the position of the seed point used in [31]. The yielded pathways traverse superiorly through the posterior limb of the internal capsule and form the corona radiata, consistent with the route of the corticospinal tract. It is also apparent that the computed course of the fiber tract from the start point branches into a couple of different cortical motor regions, including the

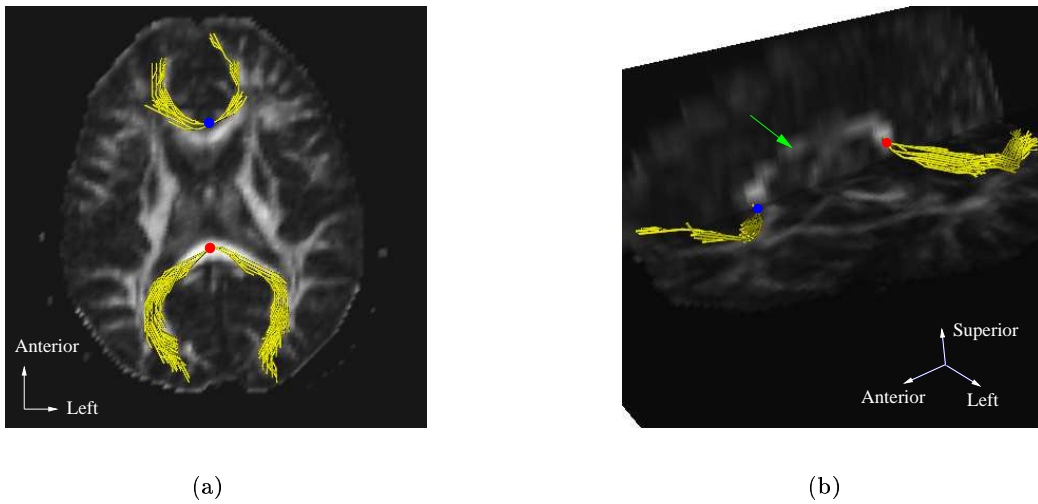
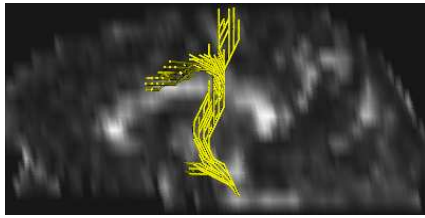
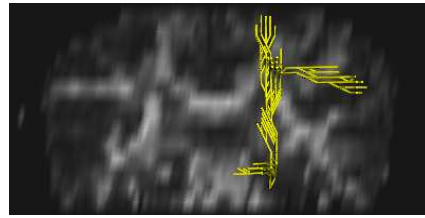


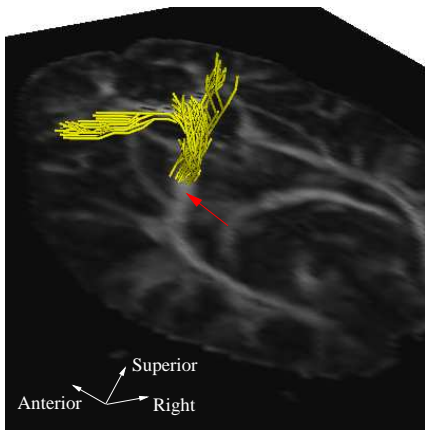
Figure 7: Fiber pathways of corpus callosum computed from two start voxels located in the genu and splenium of the corpus callosum (green arrow), as labeled by blue and red circle, respectively. Fibers are incorporated into grey-scale fractional anisotropy (fa) maps for anatomical reference, where bright grey-scale regions reflect high diffusion anisotropy. (a) Fibers are viewed from the inferior direction, overlaid on an axial fa map. (b) Fibers are viewed from above in the anterior-left direction, shown together with a midline sagittal fa map as well as an axial one.



(a)



(b)



(c)

Figure 8: Fiber pathways of corticospinal tract computed from a start voxel positioned approximately in the left portion of the base of the pons area. (a) Viewed from left, overlaid on a sagittal fractional anisotropy (fa) map at the midline, showing the tract branching into the primary and supplementary motor regions and the premotor cortex. (b) Viewed from front, superimposed on a coronal fa map, showing the projection pathways diverging into the medial and lateral primary motor areas of the left hemisphere. (c) A 3D view, shown together with an axial fa map, showing the fibers passing superiorly through the posterior limb of the internal capsule, as pointed by the red arrow, and forming the corona radiata.

medial and lateral parts of the primary motor cortex, the supplementary motor area, and the premotor cortex, as shown in Figure 8. The projections to the pons area from the motor regions via the estimated corticospinal tract are in good agreement with the known anatomical and functional connections and are similar to those obtained in [23, 30, 31] as well.

The third demonstration for the fiber tracking conducted by our diffusion simulation based tractography algorithm is to replicate the tract of optic radiations, or geniculocalcarine visual projection, that relays visual information from the lateral geniculate nucleus (LGN) of the thalamus to the visual cortex. Two start points, one for each of the cerebral hemisphere, are placed in the body of the optic radiations, lateral to the position of the LGN, similar to those chosen in [30]. The computed fibers of the optic radiations are displayed in Figure 9, showing that each optic radiation arises from the start voxel, sweeps posteriorly through the temporal lobe then the occipital lobe, and terminates in

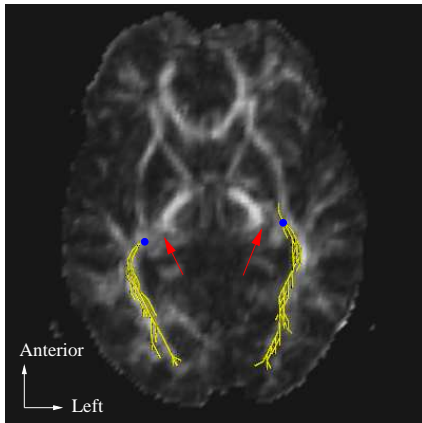


Figure 9: Fiber pathways in the optic radiations, from two start voxels (blue circles) lateral to each of the lateral geniculate nucleus (LGN). Fibers are viewed from the inferior direction, overlaid on an axial fractional anisotropy (fa) map for anatomical reference. The approximate positions of the LGN are shown by red arrows.

the region of the calcarine sulcus with branching traces. The characteristic topology of the optic radiation is known to be that its spatial course runs in a medial-lateral orientation after coming out of the LGN and then changes to an anterior-posterior orientation, which is demonstrated by the tract behavior in [11, 30, 31]. However, the portion of the optic radiation that runs in the medial-lateral direction between the LGN and the start points is not identified in the current tracking result obtained by our fiber tracking algorithm. The reason for the difficulty in this case is likely due to the coarse resolution in the superior-inferior direction of the original DT-MRI data set we are currently relying on, and the interpolated data actually used in the demonstration is also unable to make contributions to tracking the sharp turning area with high curvature in the optic radiation. A further investigation on this issue is being carried out.

Figure 10 shows the result of the last tractography experiment with our tracking scheme applied, in which we trace one of the long association pathways, the tract of the inferior occipitofrontal fasciculus. The position of the start voxel is located approximately in the junction area of the frontal and temporal lobes in the left hemisphere, from which the generated fasciculus fans out in both anterior and posterior directions. On one hand, the fasciculus runs anteriorly, radiating into cortical regions of the frontal lobe. On the other hand, it streams backward, branching into the temporal and occipital lobes. Apparently, the reproduced tract of the inferior occipitofrontal fasciculus connects the frontal cortex with the posterior temporal cortex and the occipital lobe, which is similar to those obtained in [10, 23].

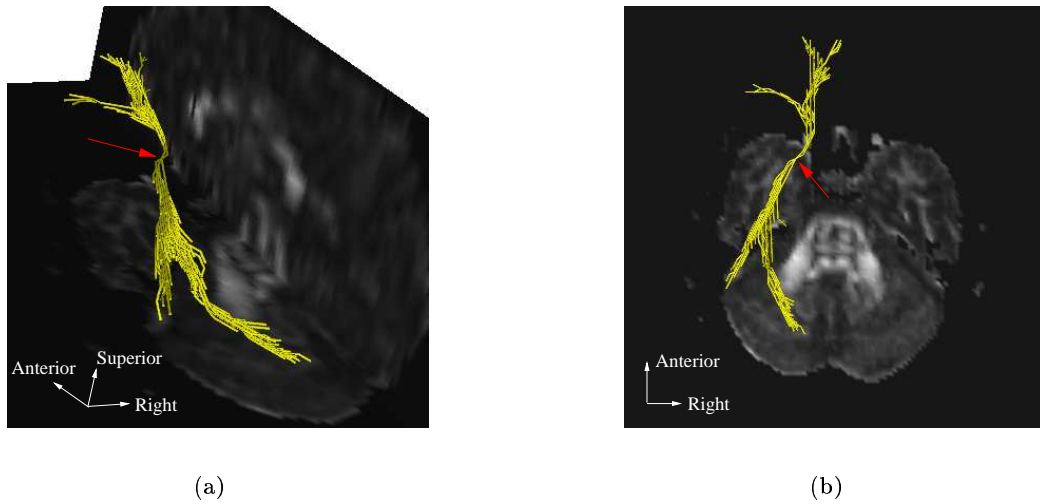


Figure 10: Fiber pathways in the inferior occipitofrontal fasciculus, emerging from a start voxel (indicated by the red arrow) in the junction area of the frontal and temporal lobes in the left hemisphere. (a) A 3D view, shown together with an axial as well as a midline sagittal fractional anisotropy (fa) map. (b) Viewed from above, overlaid on an axial fa map.

4 Discussion

We have presented the tractography results utilizing the diffusion-simulation based fiber tracking algorithm for diffusion tensor MRI data. The tracking experiments have been performed on the corpus callosum commissural fibers, the corticospinal tract, the optic radiation, and the inferior occipitofrontal fasciculus, and the estimated pathways are largely faithful to the corresponding neuroanatomy performed with postmortem dissections [17, 44] and compatible to those obtained by using other tracking approaches, such as streamline-based tractography [3, 10, 11, 23, 45] and fast marching tractography [30, 31]. The demonstration shows that with the diffusion tensor imaging data, it is possible to employ the diffusion-based tracking technique to noninvasively reconstruct the major white matter fiber trajectories in the living human brain.

Previous work, as shown in [4, 13, 27], has attempted to create time-of-arrival maps of a diffusion front by solving simplified variants of the general anisotropic diffusion equation (3). In the approach proposed in [4], a seed diffuses through the brain from a selected starting point by solving the full diffusion equation and the amount of concentration at some location is interpreted as a probability to reach that point. The work of [27] instead solves the steady-state diffusion equation with boundary conditions of one source and one sink and then uses this information to calculate the steady-state flow field which is supposed to recover the underlying anatomical path between the source and sink. Both methods are completely different from our way to exploit the diffusion process, in which

we construct successive three dimensional diffusion fronts to determine the fiber pathways by evaluating the distance and orientation from the computed fronts to their analogous diffusion seeds. In [13], a simplified version of the anisotropic diffusion equation (3) is solved, however, no effort has been made to show that the paths of fibers or the connections can be reconstructed between anatomical or functional regions of the brain.

Regarding the use of diffusion tensor data for unveiling the organizational patterns of white matter structures, our diffusion-based tractography has two potential advantages. First, as we have demonstrated, it has the capability to elucidate branching pathways naturally like the fast-marching approach, which is an advantage compared to the streamline type methods. As noticed in [31], without using some schemes such as making multiple interpolated start points within the start voxel, it is impossible for the existing streamline-based tracking methods to generate diverging fiber trajectories when the tracing starts from a single point, while with the use of these schemes, the density of trajectories will reduce and thus get subsequent connected regions undersampled. There is no such undersampling problem for the branching process in our tractography since the algorithm follows all branching pathways in the same manner, computing diffusion fronts consecutively. The fast marching tractography developed in [30, 31] also presents the desired feature to allow tract branching, in which the fast marching technique is adopted in the context of the diffusion tensor field to propagate fronts that evolve at a rate controlled by the information contained in the principal eigenvector field. Compared to the fast marching approach, our diffusion-based tractography relies on simulating the diffusion process to construct successive diffusion fronts, and more importantly, the diffusion simulation is more problem-oriented than the level set methods which are more general purpose vehicles.

The second feature of our method is that it is likely to enhance the robustness and reliability in fiber reconstruction. Used as the basis for our tractography, performing simulations on the diffusion process, which is truly a physical phenomenon, is evident to help reveal the underlying tissue structures. Therefore we are able to utilize the diffusion distance measure to construct the fiber trajectory, instead of fully banking on the orientation of the tensor in each voxel. As mentioned earlier, the noise of the imaging system will add uncertainty to the estimation of the diffusion tensor field and its eigenvectors. This effect will yield an accumulation of orientational errors and thus spurious trajectories when tracing the white matter tracts solely depends on the information contained in the principal eigenvector field, as most of the streamline-based tracking methods and the fast marching tractography do. Our diffusion-based tractography, however, has a lower chance to get affected by the noise since more information from the diffusion simulation is involved in determining the fiber pathways, helping partially restrain the problem, although we do use the principal eigenvector to regulate the path curvature.

Since our tractography process spreads diffusion over the brain regardless of whether an area has high or low anisotropy values, it is possible for the method to get through regions with low anisotropy to find pathways, and thus to avoid dropouts (premature interrupts) of fiber tracking, partly overcoming the partial volume effects. But it needs further investigation and demonstration. Although the diffusion-based technique has this

potential, it is difficult to validate the accuracy of crossing fibers and rule out the possibility of false fiber courses. Another limitation of our method is that the spatial resolution of the measured diffusion tensor data likely affects the ability to track small fiber tracts and the fiber bundles with high curvatures, as in the reconstruction of the optic radiation. However, the spatial resolution is not a problem specific to our approach. What is deserved to take a closer look is that whether it is more critical to our approach than to other techniques, such as the streamline-based methods.

In the current paper, our tracking algorithm is demonstrated by showing data from only one subject. But we are going to obtain and report results across a few more different subjects to increase the confidence in the performance of the diffusion-based tractography. The investigation and evaluation of the pathway connection criteria will also be included in the future work as well as the development of connectivity likelihood measures. In addition, the timing for the current algorithm is a little bit long, running a couple of hours for a typical case, since we have to carry out a diffusion simulation for each of the diffusion roots and each of the simulations sweeps the whole brain volume. The improvement for the algorithm on computation time has been under way, in which each diffusion simulation initiated from a root only spreads through its neighboring parts of the brain, expected to drastically reduce the running time.

5 Conclusion

In summary, a novel white matter fiber tractography algorithm is developed using diffusion tensor MRI data. This technique is based on conducting consecutive simulations of anisotropic diffusion over the living human brain, which are utilized to construct three dimensional diffusion fronts. The fiber trajectories are constructed by evaluating the distance and orientation from fronts to their corresponding diffusion seeds. The demonstration shows the reconstruction of several major white matter fiber pathways, which seem reasonable in comparison with the known anatomy and largely similar to those estimated by using other tracking approaches. The ability to yield branching pathways is the primary advantage of the diffusion-based tractography presented in this work and it also has the potential to enhance robustness and reliability in the fiber tractography process.

References

- [1] B. A. Ardekani, J. Nierenberg, M. J. Hoptman, D. C. Javitt, and K. O. Lim, MRI study of white matter diffusion anisotropy in schizophrenia, *Neuroreport*, 14(16):2025-9, Nov 2003.
- [2] P.J. Basser, J. Mattiello, and D. Le Bihan, Estimation of the effective self-diffusion tensor from the NMR spin echo, *Journal of Magnetic Resonance*, Series B, 103:247-254, 1994.

- [3] P.J. Basser, S. Pajevic, C. Pierpaoli, J. Duda, and A. Aldroubi, In vivo fiber tractography using DT-MRI data, *Magnetic Resonance in Medicine*, 44:625-632, 2000.
- [4] P.G. Batchelor, D.L.G. Hill, F. Calamante, and D. Atkinson, Study of connectivity in the brain using the full diffusion tensor from MRI, M.F. Insana, R.M. Leahy (Eds.): *IPMI 2001, Lecture Notes in Computer Science 2082*, pp.121-133, 2001.
- [5] P.G. Batchelor, D.L.G. Hill, D. Atkinson, F. Calamante, and A. Connelly, Fibre-tracking by solving the diffusion-convection equation, *Proceedings of the International Society for Magnetic Resonance Medicine*, 2002.
- [6] C. Beaulieu, The basis of anisotropic water diffusion in the nervous system - a technical review, *NMR in Biomedicine*, 15:435-455, 2002.
- [7] M. Björnemo and A. Brun, R. Kikinis, and C.F. Westin, Regularized stochastic white matter tractography using diffusion tensor MRI, *MICCAI*, Tokyo, Japan, September, 2002.
- [8] F. Calamante, D.A. Porter, D.G. Gadian, and A. Connelly, Correction for eddy-current induced B_0 shifts in diffusion-weighted echo-planar imaging, *Magnetic Resonance in Medicine*, 41(1):95-102, 1999.
- [9] J.S.W. Campbell, K. Siddiqi, B.C. Vemuri, and G.B. Pike, A geometric flow for white matter fibre tract reconstruction, *Proceedings of IEEE International Symposium on Biomedical Imaging Conference*, pp.505-508, July 2002.
- [10] M. Catani, R.J. Howard, S. Pajevic, and D.K. Jones, Virtual in vivo interactive dissection of white matter fasciculi in the human brain, *NeuroImage*, 17:77-94, 2002.
- [11] T.E. Conturo, N.F. Lori, T.S. Cull, E. Akbudak, A.Z. Snyder, J.S. Shimony, R.C. McKinstry, H. Burton, and M.E. Raichle, Tracking neuronal fiber pathways in the living human brain, *Proceedings of the National Academy of Sciences of USA*, Vol. 96: 10422-10427, August 1999.
- [12] J. Foong, M. Maier, C.A. Clark, G.J. Barker, D.H. Miller, and M.A. Ron, Neuropathological abnormalities of the corpus callosum in schizophrenia: a diffusion tensor imaging study, *Journal of Neurology, Neurosurgery, and Psychiatry*, 68(2):242-4, 2000.
- [13] D. Gembris, H. Schumacher, and D. Suter, Solving the diffusion equation for fiber tracking in the living human brain, *Proceedings of the International Society for Magnetic Resonance Medicine (ISMRM)*, 9:1529, Glasgow, Scotland, April 2001.
- [14] C. Gössl, L. Fahrmeir, B. Pütz, L.M. Auer, and D.P. Auer, Fiber tracking from DTI using linear state space models: detectability of the pyramidal tract, *NeuroImage*, 16:378-388, 2002.

- [15] M. Guye, G.J.M. Parker, M. Symms, P. Boulby, C.A.M. Wheeler-Kingshott, A. Salek-Haddadi, G.J. Barker, and J.S. Duncana, Combined functional MRI and tractography to demonstrate the connectivity of the human primary motor cortex in vivo, *NeuroImage*, 19: 1349-1360, 2003.
- [16] P. Hagmann, J.P. Thiran, L. Jonasson, P. Vandergheynst, S. Clarke, P. Maeder, and R. Meuli, DTI mapping of human brain connectivity: statistical fibre tracking and virtual dissection, *NeuroImage*, 19:545-554, 2003.
- [17] J. Hanaway, *The Brain Atlas: a Visual Guide to the Human Central Nervous System*. Bethesda, Maryland: Fitzgerald Science Press, 1998.
- [18] L. Jonasson, P. Hagmann, X. Bresson, R. Meuli, O. Cuisenaire, and J.-P. Thiran, White matter mapping in DT-MRI using geometric flows, *Proceedings of the 9th International Workshop on Computer Aided Systems Theory*, pp.80-82, Las Palmas de Gran Canaria, Spain, 2003.
- [19] D.K. Jones, A. Simmons, S.C.R. Williams, and M.A. Horsfield, Non-invasive assessment of axonal fiber connectivity in the human brain via diffusion tensor MRI, *Magnetic Resonance in Medicine*, 42:37-41, 1999.
- [20] N. Kang, J. Zhang, and E.S. Carlson, Performance of ILU preconditioning techniques in simulating anisotropic diffusion in the human brain, *Future Generation Computer Systems*, 20(4):687-698, 2004.
- [21] N. Kang, J. Zhang, and E.S. Carlson, Parallel simulation of anisotropic diffusion with human brain DT-MRI data, *Computers and Structures*, accepted.
- [22] M.A. Koch, D.G. Norris, and M. Hund-Georgiadis, An investigation of functional and anatomical connectivity using magnetic resonance imaging, *NeuroImage*, 16:241-250, 2002.
- [23] M. Lazar, D.M. Weinstein, J.S. Tsuruda, K.M. Hasan, K. Arfanakis, M.E. Meyerand, B. Badie, H.A. Rowley, V. Haughton, A. Field, and A.L. Alexander, White matter tractography using diffusion tensor deflection, *Human Brain Mapping*, 18:306-321, 2003.
- [24] D. Le Bihan, J.F. Mangin, C. Poupon, C.A. Clark, S. Pappata, N. Molko, and H. Chabriat, Diffusion tensor imaging: concepts and application, *Journal of Magnetic Resonance Imaging*, 13:534-546, 2001.
- [25] S. Mori, B. Crain, V.P. Chacko, and P.C.M. van Zijl, Three dimensional tracking of axonal projections in the brain by magnetic resonance imaging, *Annals of Neurology*, 45:265-269, 1999.
- [26] C. Nicholson, Diffusion and related transport mechanism in brain tissue, *Reports on Progress in Physics*, 64:815-884, 2001.

- [27] L. O'Donnell, S. Haker, C.F. Westin, New approaches to estimation of white matter connectivity in diffusion tensor MRI: elliptic PDEs and geodesics in a tensor-warped space, *MICCAI*, Tokyo, Japan, September, 2002.
- [28] S. Pajevic, A. Aldroubi, and P.J. Basser, A continuous tensor field approximation of discrete DT-MRI data for extracting microstructural and architectural features of tissue, *Journal of Magnetic Resonance*, 154:85-100, 2002.
- [29] G.J.M. Parker and D.C. Alexander, Probabilistic Monte Carlo based mapping of cerebral connections utilising whole-brain crossing fibre information, In C.J. Taylor & A. Noble (Eds.): Information Processing in Medical Imaging (IPMI'03), *Lecture Notes in Computer Science*, 2737, 684-695, 2003.
- [30] G.J.M. Parker, K.E. Stephan, G.J. Barker, J.B. Rowe, D.G. MacManus, C.A.M. Wheeler-Kingshott, O. Ciccarelli, R.E. Passingham, R.L. Spinks, R.N. Lemon, and R. Turner, Initial demonstration of in vivo tracing of axonal projections in the macaque brain and comparison with the human brain using diffusion tensor imaging and fast marching tractography, *NeuroImage*, 15:797-809, 2002.
- [31] G.J.M. Parker, C.A.M. Wheeler-Kingshott, and G.J. Barker, Estimating distributed anatomical connectivity using fast marching methods and diffusion tensor imaging, *IEEE Transactions on Medical Imaging*, 21(5):505-512, May 2002.
- [32] C. Pierpaoli and P.J. Basser, Toward a quantitative assessment of diffusion anisotropy, *Magnetic Resonance Medicine*, 36:893-906, 1996.
- [33] E. Plante and L. Turkstra, Sources of error in the quantitative analysis of MRI scans, *Magnetic Resonance Imaging*, 9(4):589-95, 1991.
- [34] C. Poupon, C.A. Clark, V. Frouin, J. Régis, I. Bloch, D. Le Bihan, and J. Mangin, Regularization of diffusion-based direction maps for the tracking of brain white matter fascicles, *NeuroImage*, 12(2):184-95, 2000.
- [35] C. Poupon, J.F. Mangin, C.A. Clark, V. Frouin, J. Régis, D. Le Bihan, and I. Bloch, Towards inference of human brain connectivity from MR diffusion tensor data, *Medical Image Analysis*, 5:1-15, 2001.
- [36] S.E. Rose, F. Chen, J.B. Chalk, F.O. Zelaya, W.E. Strugnell, M. Benson, J. Semple, and D. Doddrell, Loss of connectivity in Alzheimer's disease: An evaluation of white matter tract integrity with colour coded MR diffusion tensor imaging, *Journal of Neurology, Neurosurgery, and Psychiatry*, 69:528-530, 2000.
- [37] E.O. Stejskal and J.E. Tanner, Spin diffusion measurements: spin echoes in the presence of a time-dependent field gradient, *Journal of Chemical Physics*, 42(1):288-292, 1965.

- [38] B. Stieltjes, W.E. Kaufmann, P.C.M. van Zijl, K. Fredericksen, G.D. Pearlson, M. Solaiyappan, and S. Mori, Diffusion tensor imaging and axonal tracking in the human brainstem, *NeuroImage*, 14:723-735, 2001.
- [39] B. Stieltjes, M. Schluter, H.K. Hahn, T. Wilhelm, and M. Essig, Diffusion tensor imaging: Theory, sequence optimization and application in Alzheimer's disease, *Radiologie*, 43(7):562-565, July 2003.
- [40] D.S. Tuch, T.G. Reese, M.R. Wiegell, and V.J. Wedeen, Diffusion MRI of complex neural architecture, *Neuron*, 40:885-895, 2003.
- [41] S.K. Warfield, F. Talos, A. Tei, A. Bharatha, A. Nabavi, M. Ferrant, P.M. Black, F.A. Jolesz, and R. Kikinis, Real-time registration of volumetric brain MRI by biomechanical simulation of deformation during image guided neurosurgery, *Computing and Visualization in Science*, 5:3-11, 2002.
- [42] D. Weinstein, G. Kindlmann, and E. Lundberg, Tensorlines: advection-diffusion based propagation through diffusion tensor fields, *Proceedings of IEEE Visualization*, pp.249-253, San Francisco, CA, 1999.
- [43] M.R. Wiegell, H.B. Larsson, and V.J. Wedeen, Fiber crossing in human brain depicted with diffusion tensor MR imaging, *Radiology*, 217:897-903, 2000.
- [44] T.H. Williams, N. Gluhbegovic, and J.Y. Jew, *The Human Brain: Dissections of the Real Brain*. The University of Iowa: Virtual Hospital, 1999. <http://www.vh.org/adult/provider/anatomy/BrainAnatomy/BrainAnatomy.html>.
- [45] D. Xu, S. Mori, M. Solaiyappan, P.C.M. van Zijl, and C. Davatzikos, A framework for callosal fiber distribution analysis, *NeuroImage*, 17:1131-1143, 2002.
- [46] L. Zhukov and A.H. Barr, Oriented tensor reconstruction: tracing neural pathways from diffusion tensor MRI, *Proceedings of IEEE Visualization*, Boston, MA, 2002.